Available online at www.sciencedirect.com
SCIENCE DIRECT®
International Journal of Thermal Sciences 43 (2004) 733–741
International Journal of Thermal Sciences
www.elsevier.com/locate/ijts

Heat transfer due to unsteadily impinging jets

Heinz Herwig [a,*], Horst Mocikat [a], Thomas Gürtler [b], Stefan Göppert [b]

[a] *TU Hamburg–Harburg, 21073 Hamburg, Germany*
[b] *TU Chemnitz, 09107 Chemnitz, Germany*

Received 20 August 2003; received in revised form 7 January 2004; accepted 24 February 2004

Available online 9 June 2004

Abstract

In a systematic experimental study the heat transfer under three different periodically unsteady jets is compared to that of the corresponding steady inline jet. Unsteadiness of the jets is created by vortex shedding (Karman jet nozzle), alternating flow passages (flip–flop nozzle) as well as by a precessing motion of the whole jet (precessing jet nozzle).

The unsteadiness of the jets is self-sustained, i.e., there are no external (mechanical) means and no external energy input to create unsteadiness. Heat transfer data in terms of Nusselt numbers are determined on a specially designed heat transfer plate in the plane of jet impingement.

Whilst there is a slight increase in heat transfer performance when vortex shedding occurs within the jet (Karman jet nozzle), in both other cases there is a considerable decrease in heat transfer.

Keywords: Jet impingement; Unsteady flow; Precessing flow; Karman vortex street; Flip–flop nozzle

1. Introduction

Convective heat transfer is one of the technically important modes of exchanging internal energy between a solid body and its ambient, either for cooling or heating purposes. The rate of heat transfer in this process strongly depends on the flow field, its strength as well as its structure, with appropriate nondimensional heat transfer coefficients covering several orders of magnitude, when the flow field parameters are changed within reasonable ranges.

A standard situation in convective heat transfer is an impinging jet on a plane surface in an otherwise quiescent ambient. This arrangement is often used for body cooling. Due to the analogy of convective heat and mass transfer it is also important for drying processes.

Though the geometry of the jet/plate combination is quite simple there are nevertheless a large number of parameters in this convective heat transfer arrangement, like: nozzle to plate distance, *Re* number, turbulence level, nozzle inclination angle (if not vertical), wall roughness, just to mention a few. All these parameters affect the heat transfer performance of the arrangement and can be changed systematically in order to influence the rate of heat transfer. The vast body of literature dealing with special aspects is well documented in review articles like [1–3].

Within the special means by which impinging jet heat transfer can be manipulated unsteadiness of the flow field is rarely used. However, unsteady flows are distinctly different compared to their steady counterparts, so that there should be a high potential to affect the heat transfer performance of such flows. Studies about the influence of unsteady flow fields on convective heat transfer almost always generate the unsteady flow by external means like forced pulsation or periodic interruption of the jet impingement. Typical studies of this kind are [4–7], with no general trend in the results: some find enhanced heat transfer, some do not.

Our approach, however, is a self-sustained unsteadiness without external input of energy and without moving parts in the system providing the flow field for convective heat transfer. We use "classical" ways to achieve this: (1) the famous von Karman vortex street behind a circular cylinder in cross flow, (2) the flow through a flip–flop fluidic element (alternating flow in a Y-shaped conduct). A less well-known

* Corresponding author. Fax: +49-40-42878-4169
E-mail address: h.herwig@tuhh.de (H. Herwig).

1290-0729/$ – see front matter
doi:10.1016/j.ijthermalsci.2004.02.013

Nomenclature

A	surface	m^2
D	diameter	m
f	frequency	s^{-1}
h	nozzle height	m
H	nozzle/plate distance	m
k	thermal conductivity	$W{\cdot}m{\cdot}K^{-1}$
Nu	Nusselt number, Eq. (1)	
p	pressure	$N{\cdot}m^{-2}$
$\dot{q}$	heat flux density	$W{\cdot}m^{-2}$
R	radial distance	m
R	electric resistance	Ω
Re	Reynolds number	
Sr	Strouhal number	
T	temperature	K
U	voltage	V
w	velocity	$m{\cdot}s^{-1}$
z_R	reference position	m
ν	kinematic viscosity	$m^2{\cdot}s^{-1}$

Indices

AMB	ambient
AS	air supply
c	conduction
e	electric
FC	flow control
FFN	flip–flop jet nozzle
HTS	heat transfer surface
IJN	inline jet nozzle
KJN	Karman jet nozzle
N	nozzle
PJN	precessing jet nozzle
r	radiation
R	reference
RMS	root mean square
SF	single field
SF0	single field of temperature T_0
SH	shunt
W	wall

configuration is that of a nozzle which due to its special shape results in a periodically precessing jet (our case (3)).

The objective of our study is to find out how strong convective heat transfer is influenced by the unsteady motion of the impinging jet, what are the crucial parameters of the configuration with respect to heat transfer and whether there is a potential for heat transfer augmentation. There are some aspects in favour of transfer augmentation like the fact that an unsteadily impinging jet results in a permanent boundary layer renewal. But there are also negative aspects like an increased mixing of the jet with the ambient fluid which reduces the jets maximum velocities and hence the good transfer properties of a narrow, high velocity jet. What is the overall effect is one of the questions that should be answered by our study.

2. Unsteady jets without moving parts; nozzle design

Unsteady jets without moving parts and without additional energy input are attractive with respect to maintenance and running costs once they are implemented in an apparatus that operates permanently or at least frequently.

The three different nozzle designs of our study together with their main geometric parameters will be introduced in the following sub-sections.

2.1. The Karman jet nozzle (KJN)

The von Karman vortex street behind an object with circular cross section introduces a periodic or quasi-periodic character into an otherwise steady jet by periodic vortex shedding. Since our jet is axisymmetric we created vortex shedding at a ring perpendicular to the main flow direction.

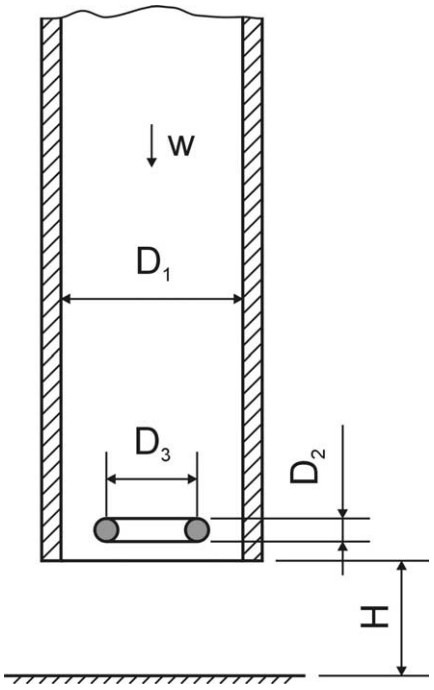

Fig. 1. Karman jet nozzle parameter specification: $D_1 = 47$ mm; $D_2 = 6$ mm; $D_3 = 26$ mm.

Fig. 1 shows the principle design of such a nozzle together with some geometrical details. Once the nozzle geometry is fixed the crucial parameters are:

- Nozzle to plate distance: H/D_1;
- Reynolds number: $Re_{KJN} = wD_1/\nu$.

The reference case (steady flow) is that through the same nozzle but without the vortex generating ring.

2.2. The flip–flop nozzle (FFN)

Within a square cross section a plane jet emerging from the narrow central slit can either attach to the left or to the right wall on the way through the nozzle. The jet attachment to an adjacent wall is known as Coanda effect. If now both sides of the nozzle are connected by an external tube of length L pressure signals can travel between both sides and, provided they are properly designed in length, can influence the attached jet so that is switches between both sides with a certain finite frequency. This arrangement is called flip–flop nozzle and produces a highly unsteady jet.

Fig. 2 shows the principle design together with some geometrical details. With a fixed geometry within the nozzle the crucial parameters of this arrangement are

- Length of the external tube: L/A; within certain limits the frequency of the flip–flop motion can be changed by changing the tube length;
- Nozzle to plate distance: H/B;
- Reynolds number: $Re_{\mathrm{FFN}} = wB/\nu$.

The reference case (steady flow) is the same nozzle without the triggering tube and with the dark grey parts removed (see Fig. 2).

2.3. The precessing jet nozzle (PJN)

Fig. 3 shows the design of this axisymmetric nozzle. Due to slight perturbations the round jet emerging from the small orifice with diameter D_{P2} moves to the adjacent wall through a mechanism similar to the Coanda effect in plane flow. However, since there is no right/left alternative as in the plane flow a stable flow situation only occurs when the jet on his way downstream moves along the inner wall of the envelope tube with a certain azimutal velocity component, thus performing a precessing motion within the tube.

In a coordinate system fixed to the plate of the nozzle/plate configuration the flow from the nozzle impinges as a jet that periodically moves around an impingement circle. At a fixed point of the plane there thus is an unsteady (periodic) flow that will affect the convective heat transfer by this unsteadiness.

Parameter of this configuration are:

- Nozzle to plate distance: H/D_{P2};
- Reynolds number: $Re_{\mathrm{PJN}} = wD_{\mathrm{P2}}/\nu$.

The reference case (steady flow) is the mere inline jet with the envelope tube removed.

The frequency of precession depends on the absolute size of the nozzle and the Reynolds number of the flow. For the two geometries specified in the caption of Fig. 3 as case (a) and (b) we found frequencies of $f = 23.3$ Hz and $f = 30.2$ Hz for almost the same Reynolds number $Re = 5.8 \times 10^4$ and $Re = 5.6 \times 10^4$.

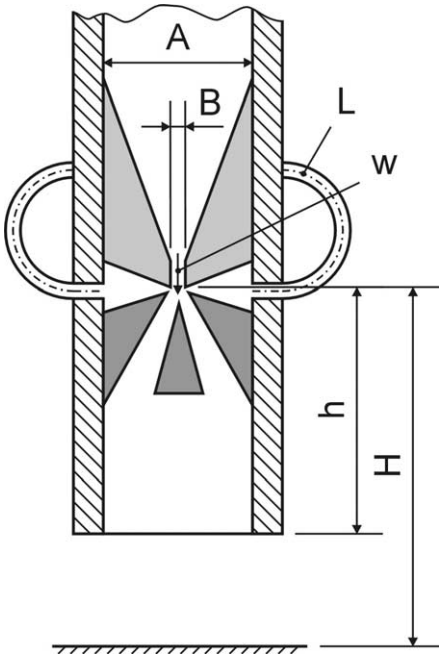

Fig. 2. Flip–flop nozzle parameter specification: $A = 40$ mm; $B = 3.5$ mm; $h = 66$ mm, $W = 40$ mm (width of the nozzle).

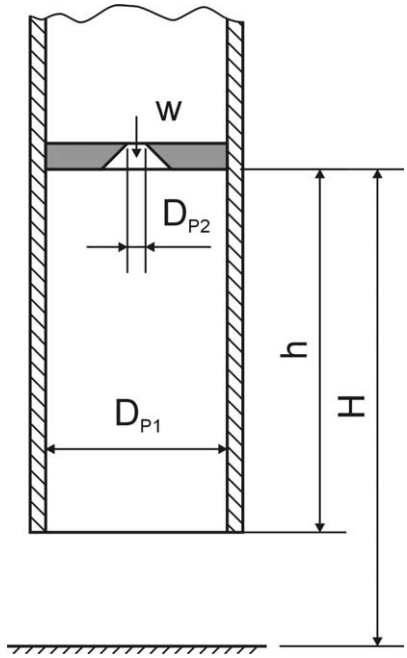

Fig. 3. Precessing jet nozzle parameter specification: (a) $D_{\mathrm{P1}} = 47$ mm; $D_{\mathrm{P2}} = 5$ mm; $h = 94$ mm, (b) $D_{\mathrm{P1}} = 35$ mm; $D_{\mathrm{P2}} = 3.5$ mm; $h = 70$ mm.

In terms of the nondimensional Strouhal number $Sr = f D_{P2}/w$ they correspond to $Sr = 8.3 \times 10^{-4}$ and $Sr = 7.8 \times 10^{-4}$, respectively.

3. The test facility

Fig. 4 is a schematic figure of our experimental design with the four main parts being the air supply, flow control, the nozzle and last but not least the heat transfer surface. Also shown are the various data that are collected during the experiments and processed in our data acquisition system. Details are:

3.1. Air supply

The air was taken from the high pressure net in our lab. A pressure reduction valve including a filter together with a precision pressure control facility provided a constant air flow of adjustable rate.

In a flow meter the pressure difference Δp_{AS} across an orifice is measured and based on the calibration of the system the actual mass flux is determined. Electrical heating of the flow is installed in this section and controlled by temperature readings from the flow control part that is described next.

3.2. Flow control

Fig. 5 shows a quieting chamber which is the flow control part of our test facility. It provides a flow to the attached nozzle with

- a nearly uniform velocity profile;
- a very low turbulence level;
- a temperature T_{FC} equal to the ambient temperature T_{AMB}.

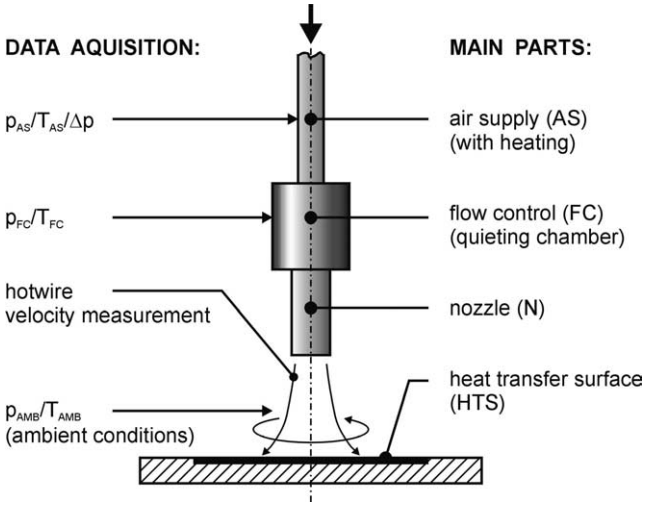

Fig. 4. Our test facility/main parts and data collected.

Based on the temperature reading in the flow control chamber the electrical heating in the upstream air supply part is controlled in order to guarantee that T_{FC} is always equal to T_{AMB}. Thus we avoid that heat transfer is affected by temperature effects in conjunction with the jet entrainment.

3.3. Heat transfer surface

From the rate by which an impinging jet cools a uniformly heated surface Nusselt numbers can easily be determined. Here the local Nusselt number Nu is defined as

$$Nu = \frac{\dot{q}_W D_i}{(T_W - T_{AMB})k} \tag{1}$$

with the local heat flux density at the wall ($\dot{q}_W$), the local wall temperature (T_W) and the characteristic diameter D_i specified for each nozzle.

Heat transfer coefficients with respect to finite parts $\hat{A}$ of the surface are

$$\overline{Nu} = \frac{\bar{\dot{q}}_W D_i}{(\overline{T}_W - T_{AMB})k} \tag{2}$$

with $\bar{\dot{q}}_W = \frac{1}{\hat{A}} \int \dot{q}_W \, dA$ and $\overline{T}_W = \frac{1}{\hat{A}} \int T_W \, dA$ as surface averaged heat flux density and temperature, respectively.

Fig. 6 sketches the design of our heat transfer plate for measuring wall heat flux densities and wall temperatures simultaneously. The main part of the heat transfer surface which has the double function of heating and measuring is an electrical circuit board with a special circuit design on both surfaces. The top surface which faces the impinging jet is covered with a densely meandering strip conductor between A and B. If there is uniform dissipation due to the electrical resistance of the conductor we thus get a local heat flux density at the wall which is almost constant (on a scale larger than the distance between two conductors). The central part of the plate is subdivided into 64 single fields

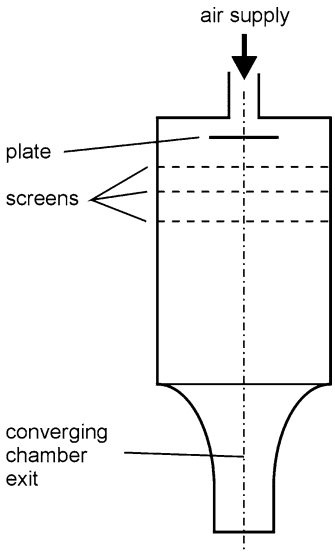

Fig. 5. Flow control in the quieting chamber.

of size $(46.8\ \text{mm})^2$ so that the whole heat transfer surface covers an area of $(374.4\ \text{mm})^2$. The grey shaded part around this surface in Fig. 6, is for additional heating in order to reduce the heat losses towards the edges of our heat transfer plate.

For each of the 64 single fields the voltage can be measured between contacts that are led through the plate and continued to the edge of it on the rear part (bottom surface) of the board by appropriate strip conductors.

If now the board is heated with a constant electrical current (typical value: $4A$) we measure the electrical current by determining the voltage U_{SH} across a resistor with $R_{\text{SH}} \approx 4\ \Omega$ and the single field voltage U_{SF}. When the whole arrangement is calibrated with respect to its temperature/electrical resistance behaviour (i.e., $R_{\text{SF}}(T)$ is known for each of the 64 single fields; R_{SF}: single field resistance; T: temperature) we find the electrical power density of a single field as

$$\bar{\dot{q}}_{\text{SF},e} = \frac{U_{\text{SF}}(U_{\text{SH}}/R_{\text{SH}})}{\hat{A}_{\text{SF}}} \tag{3}$$

From this we get the wall heat flux density $\bar{\dot{q}}_{\text{W}}$ in Eq. (2) for a single field by taking into account the additional radiation flux density

$$\bar{\dot{q}}_{\text{SF},r} = \varepsilon\sigma\left(\overline{T}_{\text{W}}^4 - T_{\text{AMB}}^4\right) \tag{4}$$

and losses by heat conduction to the rear of our heat transfer plate. With isolation foam material of thickness S_i and conductivity k_i they can be kept small and are

$$\bar{\dot{q}}_{\text{SF},c} = k_i \frac{(\Delta T)_i}{S_i} \tag{5}$$

where $(\Delta T)_i$ is the temperature difference across the isolation material.

Thus we get for $\bar{\dot{q}}_{\text{W}}$, the heat flux density of a single field in Eq. (2):

$$\bar{\dot{q}}_{\text{W}} = \bar{\dot{q}}_{\text{SF},e} - \bar{\dot{q}}_{\text{SF},r} - \bar{\dot{q}}_{\text{SF},c} \tag{6}$$

The single field temperature $\overline{T}_{\text{W}}$ can be determined as soon as the $R_{\text{SF}}(T)$ relation is known through a calibration process. For small temperature differences (like in our case) the linear ansatz $R_{\text{SF}}(T) = R_{\text{SF0}}[1 + \alpha_{\text{SF}}(T - T_0)]$ is sufficient, so that $\overline{T}_{\text{W}}$ in Eq. (2) is found as

$$\overline{T}_{\text{W}} = T_0 + \frac{R_{\text{SF}} - R_{\text{SF0}}}{\alpha_{\text{SF}} R_{\text{SF0}}} \quad \text{with } R_{\text{SF}} = R_{\text{SH}} \frac{U_{\text{SF}}}{U_{\text{SH}}}$$

By calibrating the heat transfer plate the single field coefficients α_{SF} and resistors R_{SF0} are determined. The coefficients α_{SF} differ by less than 0.2% between the 64 single fields.

So far only single field averaged quantities can be determined and the Nusselt number will be $\overline{Nu}_{\text{SF}}$ according to Eq. (2), i.e., an averaged Nusselt number for each of the 64 single fields. In order to get local values of the Nusselt number we prepared the heat transfer surface for infrared temperature measurements by coating them with black mat paint. Assuming $\dot{q}_{\text{W}}$ to be sufficiently constant across the heat transfer surface local temperature measurements by IR technique thus can give local Nusselt numbers according to Eq. (1). They compare very well with the single field averaged results, see [8].

3.4. Error analysis

In a detailed error analysis we identified and evaluated all elements of the "measuring chain" that influence the accuracy of our Nusselt number results. Based on this detailed analysis we end up with the uncertainty

$$\frac{\Delta Nu}{Nu} = \left|\frac{\Delta \dot{q}_{\text{W}}}{\dot{q}_{\text{W}}}\right| + \left|\frac{\Delta T_{\text{W}}}{T_{\text{W}} - T_{\text{AMB}}}\right| + \left|\frac{\Delta T_{\text{AMB}}}{T_{\text{W}} - T_{\text{AMB}}}\right| \tag{7}$$

assuming that D_i and k do not contribute to $\Delta Nu/Nu$.

In Fig. 7 the relative as well as the absolute uncertainties are shown for our measurements of the Nusselt numbers. Curve 1 for the relative uncertainty neglects all systematic errors and is the relevant curve when certain parameters are changed in an otherwise unchanged setting. Curve 2 includes all systematic errors and is an upper bound when it comes to a comparison with results from other studies that use

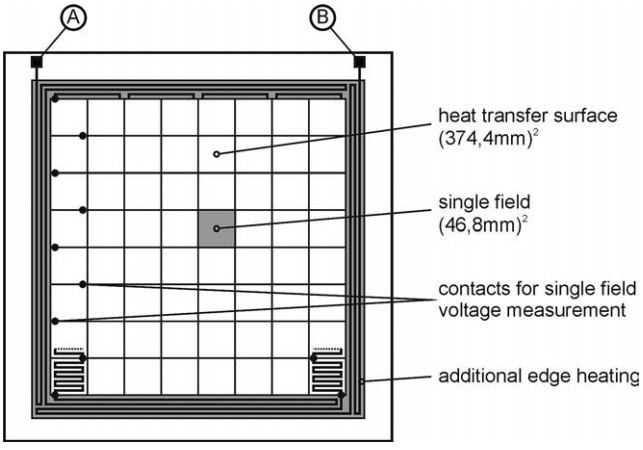

Fig. 6. Details of the heat transfer plate.

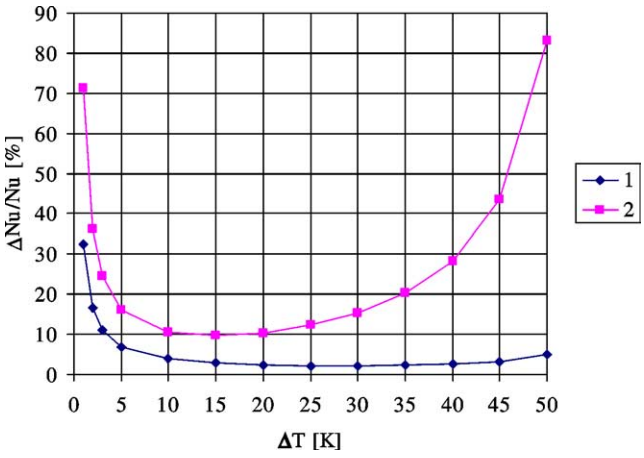

Fig. 7. Nusselt number uncertainties: curve 1: relative uncertainty (no systematic errors); curve 2: absolute uncertainty.

different measuring techniques (but with systematic errors that do not exceed our ones).

Similar considerations with respect to the Reynolds number reveal a 3% uncertainty for that quantity. From these results we conclude that our experimental set up provides data of sufficient accuracy to investigate the influence of unsteadiness on heat transfer under impinging jets.

4. Results

A crucial point in testing new nozzles is the choice of an adequate reference case. After a careful consideration of all important aspects we decided to choose a steady inline jet emerging from an orifice of diameter D_{IJN}, which was specified for three different nozzles in Section 2 already. Here IJN stands for *inline jet nozzle*. The Reynolds number of the reference case is $Re = wD_{\mathrm{IJN}}/\nu$, with w being the average velocity in the orifice.

Thus D_{IJN} for the three cases under consideration is:

- KJN: $D_{\mathrm{IJN}} = D_1$, s. Fig. 1;
- FFN: $D_{\mathrm{IJN}} = B$, s. Fig. 2;
- PJN: $D_{\mathrm{IJN}} = D_{\mathrm{P2}}$, s. Fig. 3.

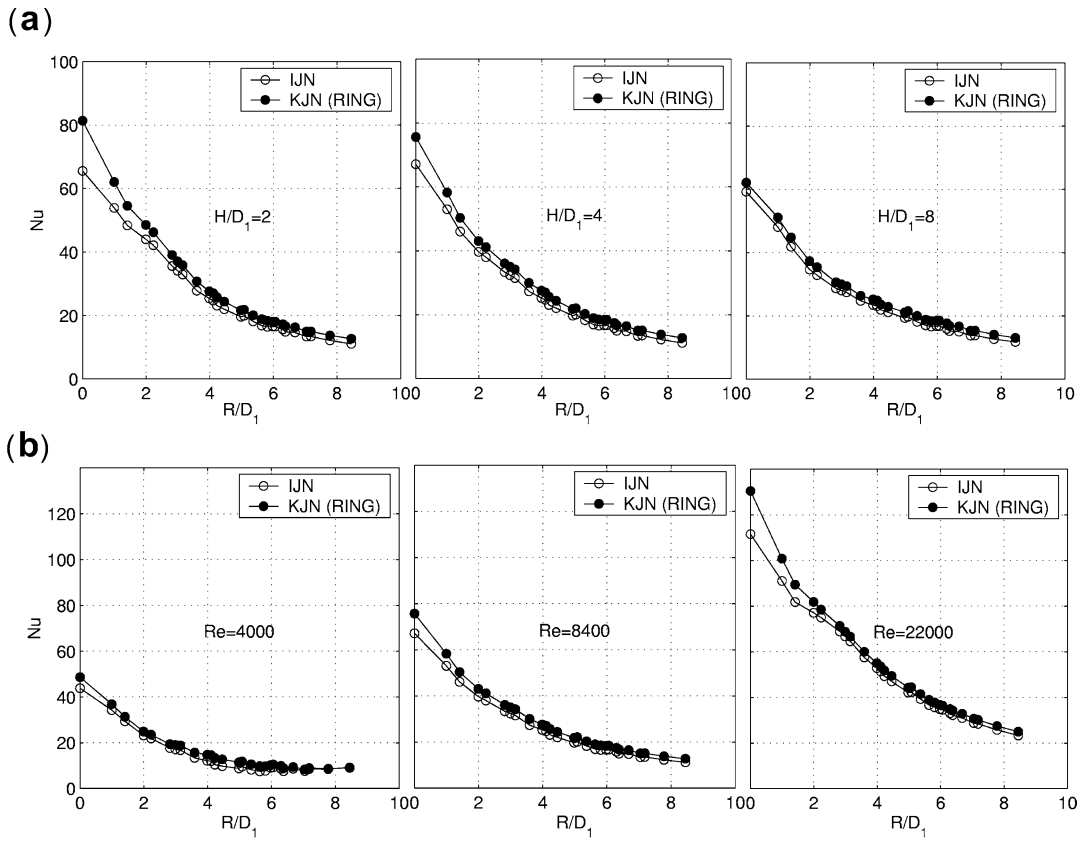

Fig. 8. Heat transfer for the Karman jet nozzle: (a) $Re = 8300$; H/D_1 variabel; (b) $H/D_1 = 4$; Re variable.

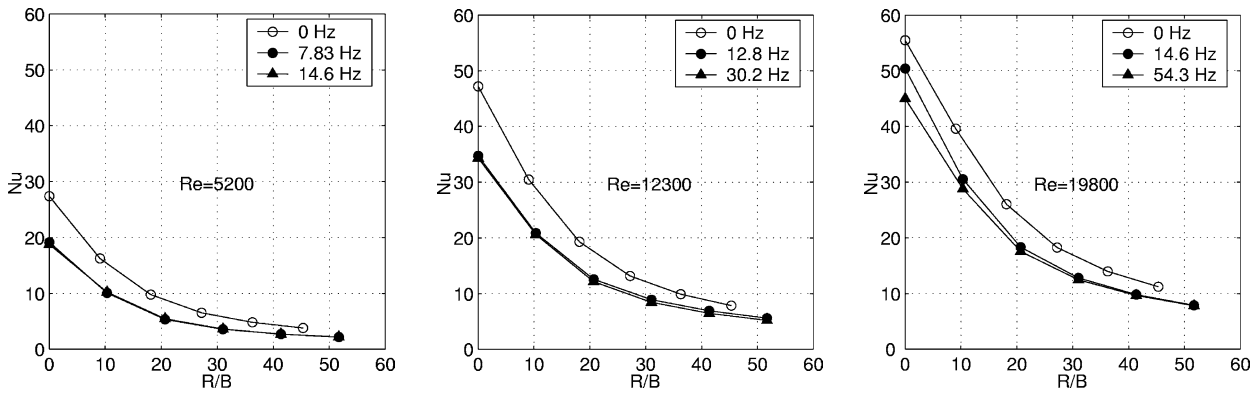

Fig. 9. Heat transfer for the flip–flop nozzle $H/B = 25$, Reynolds number as indicated.

4.1. Karman jet nozzle results

In Fig. 8 Nusselt number distributions for several parameter combinations for the Karman jet nozzle are shown (cf. Section 2.1).

The open symbols refer to the IJN-reference case with $Re_{KJN} = Re_{IJN} = Re$.

As a general trend we find a slight increase in the quasi-local Nusselt numbers for the Karman jet nozzle compared to the steady inline jet. This increase is 10–15% with the higher margins close to the stagnation point and for low values of H/D_1 as well as high values of the Reynolds number.

This increase is of the order that can be achieved by additional turbulence generation in jets so that the increase in heat transfer can be attributed to the unsteadyness of the flow field including an enhanced turbulence level.

4.2. Flip–flop nozzle results

Fig. 9 shows Nusselt number distributions for three different Reynolds numbers and a fixed nozzle to plate distance $H/B = 25$ for the flip–flop nozzle. For the unsteady flows the flip–flop frequency is given in the diagram inserts. They are influenced by the Reynolds number as well as by the length of the external tube (cf. Section 2.2) with tube lengths between 200 mm and 1500 mm for the cases shown in Fig. 9.

In Fig. 10 the Nusselt number in the vicinity of the stagnation point (i.e., at the single field around the stagnation point) is shown for various nozzle to plate distances H/B and a fixed Reynolds number $Re = 19\,800$. Again, different flip–flop frequencies occur due to different tube lengths (1500 mm for $f = 14.6$ Hz, 200 mm for $f = 54.3$ Hz).

As a general trend we find a reduction in heat transfer efficiency (i.e., in the Nusselt number) by about 20% with almost no influence of the frequency once the flip–flop

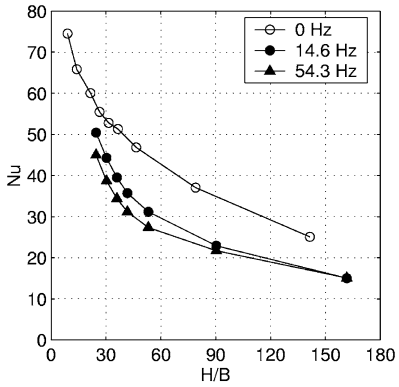

Fig. 10. Heat transfer in the stagnation region for the flip–flop nozzle versus nozzle to plate distance; $Re = 19\,800$.

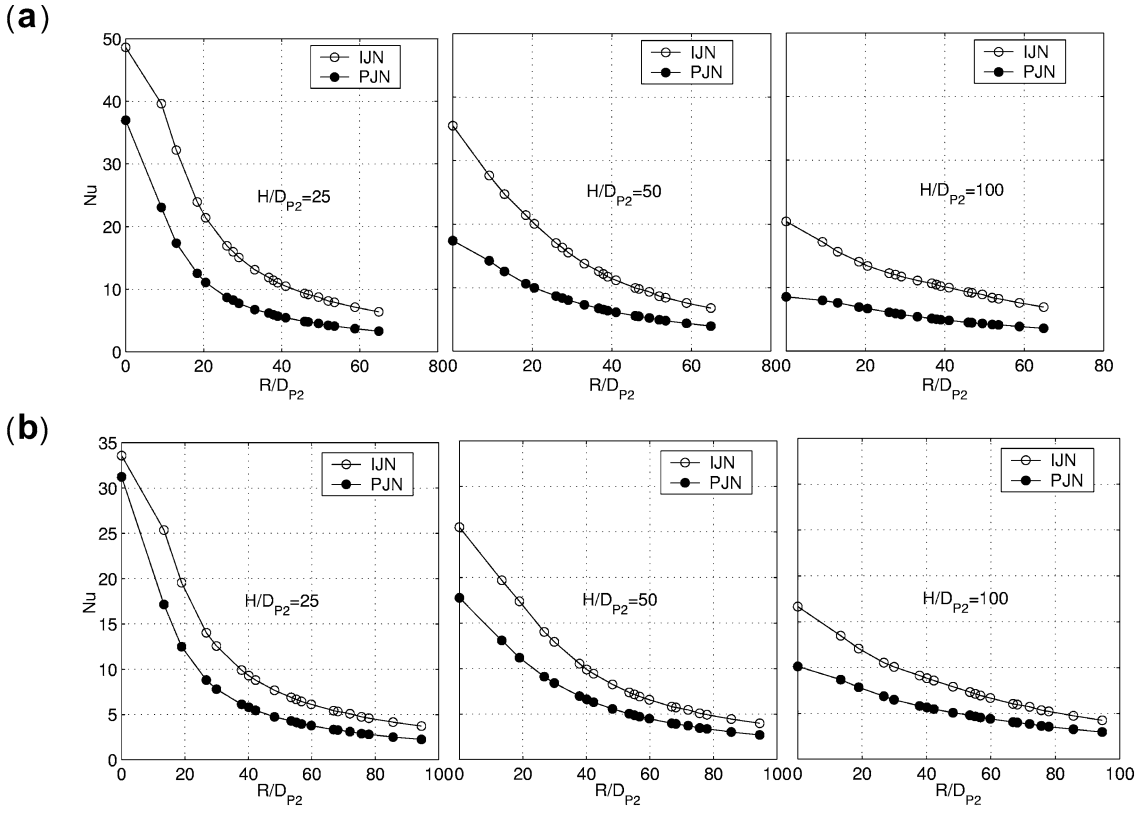

Fig. 11. Heat transfer for the precessing jet nozzle: (a) $D_{P2} = 5$ mm; $Re = 58\,000$; H/D_{P2} variable; $f = 23.3$ Hz; (b) $D_{P2} = 3.5$ mm; $Re = 56\,000$; H/D_{P2} variable; $f = 30.2$ Hz.

motion sets in. If any, there is a trend to lower heat transfer rates for higher frequencies.

4.3. Precessing jet nozzle results

Fig. 11 shows results for the precessing jet arrangement. As a general trend it turns out that the heat transfer is reduced considerably by the precessing motion. Heat transfer is reduced by almost a factor of two with no clear trend with respect to variations in the nozzle to plate distance and the precessing frequency.

Obviously the negative effect of mixing the jet with the ambient air overwhelms the positive effect of a permanent boundary layer renewal at the heat transfer surface.

In order to further reveal the physics of this flow in Fig. 12 we show the velocity and turbulence intensity distributions of the PJN case compared to the IJN reference case.

Since $z_R/D_1 = 20$ for the PJN-case is the end of the envelope tube, the velocity profile is very special there. Further downstream IJN and PJN profiles are not fundamentally different but PJN profiles are far wider spread than in-line profiles.

In Fig. 12(b) the z-dependent velocity u_R, i.e., $\bar{u}$ at $x = 0, z = z_R$, is also used to nondimensionalize the u_{RMS} values of u. Thus the ratio u_{RMS}/u_R directly shows how velocity fluctuations vary with radial distance. This ratio from our point of view is a better representation of turbulence intensity than an intensity defined with the local (i.e., z and x dependent) reference velocity that is often used.

The numbers of u_R are given in Fig. 12 for the profiles shown so that absolute values for $\bar{u}$ and u_{RMS} can be determined in the figure through the products $(\bar{u}/u_R)u_R$ and $(u_{RMS}/u_R)u_R$, respectively.

Again the PJN profiles are spread much wider with absolute values decreasing faster than in the reference case.

5. Discussion, future research

As a result of our study the following conclusions can be drawn that might be important for all those who plan to incorporate unsteady jet impingement in heat and/or mass transfer processes.

- A stable self-sustained periodic flow can be achieved by very simple means with no need for external energy or moving parts.
- Heat transfer augmentation could only be found for the Karman jet nozzle in which additional unsteadiness and turbulence is introduced without fundamentally changing the flow structure of the jet.
- The flow field with and without unsteady motion, however, can be substantially different. Velocity profiles in the unsteady case often show strong mixing of the jet with ambient fluid and thus a rapid decrease in the maximum jet velocity.

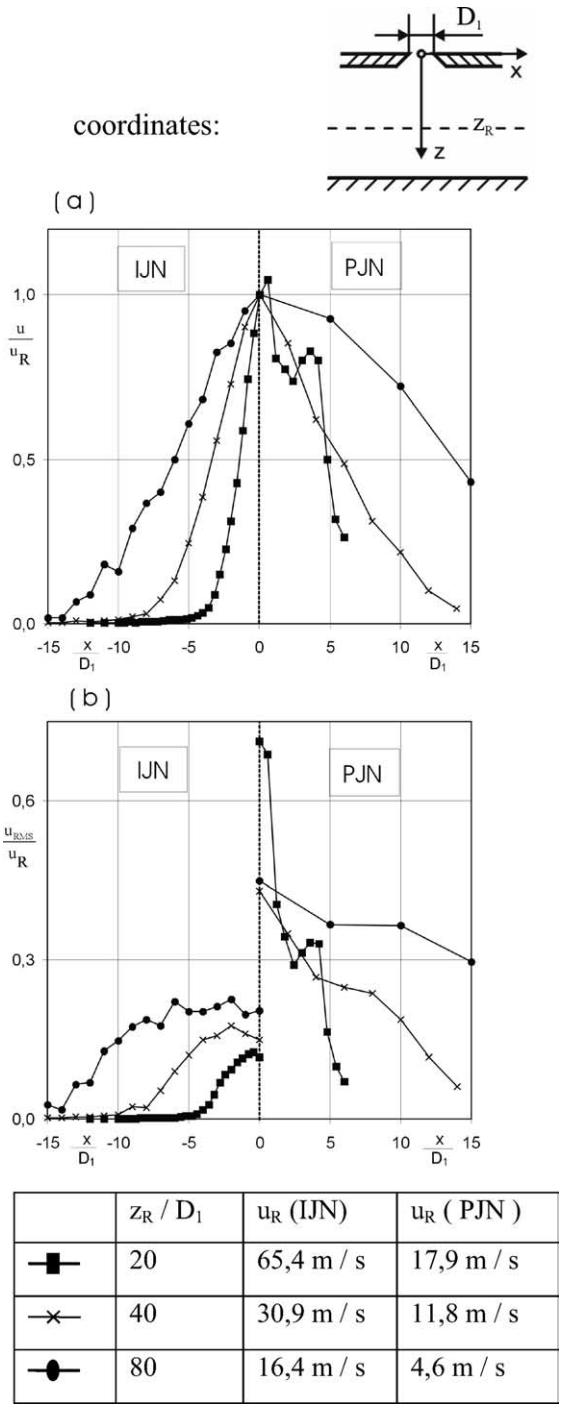

	z_R / D_1	u_R (IJN)	u_R (PJN)
■—	20	65,4 m / s	17,9 m / s
—×—	40	30,9 m / s	11,8 m / s
—●—	80	16,4 m / s	4,6 m / s

Fig. 12. Velocity and turbulence intensity profiles for the inline jet (IJN) and the precessing jet (PJN); $D_1 = 5$ mm: (a) velocity distribution u/u_R; (b) turbulence intensity distribution u_{RMS}/u_R, u_R: velocity $\bar{u}$ at $x = 0$, $z = z_R$.

- If there is rapid mixing with ambient fluid convection velocities at the heat transfer surface are relatively small and thus lead to a reduction in heat transfer. This can be stated as a general trend though the margins of reduction depend on various parameters.

Since it turned out that a prescribed self-sustained unsteadiness in general did not lead to a substantial improve-

ment in heat transfer, future research should address the question which kind of unsteadiness in the flow field increases the heat transfer performance. Then, in a second step, nozzle designs should be found that perform with the necessary kind of unsteadiness.

Acknowledgements

This study was supported by the “Deutsche Forschungsgemeinschaft” (DFG).

References

[1] H. Martin, Heat and mass transfer between impinging gas jets and solid surfaces, Adv. Heat Transfer 13 (1977) 1–60.

[2] K. Jambunathan, E. Lai, M.A. Moss, B.L. Button, A review of heat transfer data for single circular jet impingement, Internat. J. Heat Fluid Flow 13 (1992) 106–115.

[3] R. Viskanta, Heat transfer to impinging isothermal gas and flame jets, Exp. Thermal Fluid Sci. 6 (1993) 111–134.

[4] D.A. Zumbrunnen, M. Aziz, Convective heat transfer enhancement due to intermittency in an impinging jet, J. Heat Transfer 115 (1993) 91–98.

[5] L.F.A. Azevedo, B.W. Webb, M. Queiroz, Pulsed air jet impingement heat transfer, Exp. Thermal Fluid Sci. 8 (1994) 206–213.

[6] E.C. Mladin, D.A. Zumbrunnen, Local convective heat transfer to submerged pulsating jets, Internat. J. Heat Mass Transfer 40 (1997) 3305–3321.

[7] T. Liu, J.P. Sullivan, Heat transfer and flow structures in an excited circular impinging jet, Internat. J. Heat Mass Transfer 39 (1996) 3695–3706.

[8] S. Göppert, T. Gürtler, H. Mocikat, H. Herwig, Heat transfer under a precessing jet: Effects of unsteady jet impingement, Internat. J. Heat Mass Transfer 47 (2004) 2795–2806.